Aeroacoustics of T-junction merging flow

G. C. Y. Lam and R. C. K. Leung[a)]
Department of Mechanical Engineering, The Hong Kong Polytechnic University, Hung Hom, Kowloon, Hong Kong, People's Republic of China

S. K. Tang
Department of Building Services Engineering, The Hong Kong Polytechnic University, Hung Hom, Kowloon, Hong Kong, People's Republic of China

(Received 13 February 2012; revised 9 December 2012; accepted 11 December 2012)

This paper reports a numerical study of the aeroacoustics of merging flow at T-junction. The primary focus is to elucidate the acoustic generation by the flow unsteadiness. The study is conducted by performing direct aeroacoustic simulation approach, which solves the unsteady compressible Navier-Stokes equations and the perfect gas equation of state simultaneously using the conservation element and solution element method. For practical flows, the Reynolds number based on duct width is usually quite high ($>10^5$). In order to properly account for the effects of flow turbulence, a large eddy simulation methodology together with a wall modeling derived from the classical logarithm wall law is adopted. The numerical simulations are performed in two dimensions and the acoustic generation physics at different ratios of side-branch to main duct flow velocities *VR* (=0.5,0.67,1.0,2.0) are studied. Both the levels of unsteady interactions of merging flow structures and the efficiency of acoustic generation are observed to increase with *VR*. Based on Curle's analogy, the major acoustic source is found to be the fluctuating wall pressure induced by the flow unsteadiness occurred in the downstream branch. A scaling between the wall fluctuating force and the efficiency of the acoustic generation is also derived.
 [http://dx.doi.org/10.1121/1.4773351]

PACS number(s): 43.28.Ra, 43.28.Py, 43.20.Mv [AH] Pages: 697–708

I. INTRODUCTION

Mitigation of flow-induced pressure pulsations and noise is always a challenging task in many engineering applications involving fluid transporting systems. Usually these transporting systems consist of duct works with various duct elements. The major source of the air-borne noise in ducts arises from the flow unsteadiness created in the vicinity of these elements. Thus, it is essential to understand the aeroacoustics occurring at the duct elements for minimizing the noise in the fluid transporting systems.

Numerous research studies have been performed to investigate the aeroacoustic response of T-junction due to its frequent use in duct works. The aeroacoustic response is found closely linked to the acoustic resonance in the duct because the shear layer created at a T-junction may either produce or absorb the energy of the acoustic wave propagating in duct, thus promoting or inhibiting the acoustic resonance. Bruggeman[1] adopted the method of matched asymptotic expansions to determine the low-frequency acoustic response of the T-junction with grazing flow. Dequand *et al.*[2] further proposed an analytical model to improve the prediction of the pulsation amplitude of such acoustic-flow interaction. Recently, Martínez-Lera *et al.*[3] have investigated the aeroacoustic response of a T-junction numerically using the incompressible simulation, system identification technique, and Howe's energy corollary. The acoustic production was successfully captured by this approach. Karlsson *et al.*[4] adopted a 3-port model and experiments to determine the aeroacoustic properties of a T-junction under both grazing and merging flows. The prediction of whistling potential was also discussed in their work. Most of these reported works were focused on the effects of grazing flow in T-junction aeroacoustics.

One should note that the acoustic-flow interaction in aforementioned studies generally involves the potential of whistling induced by a rather high level of acoustics. This situation may not be encountered in some systems such as ventilation systems in buildings. In these cases, the noise generation by the flow unsteadiness becomes dominant. These acoustic waves propagate downstream and may induce whistling when they meet other duct elements such as T-junction. However, little research has been carried out to study the noise generation by flow unsteadiness induced in T-junction, especially in cases with a merging flow. On the other hand, the focus of the reported research of merging flow is usually put on the flow dynamics, rather than its aeroacoustics, e.g., the work of Brücker[5] in the regime of laminar flow. For higher Reynolds number flow regime, Hirota *et al.*[6] examined the merging of cold and hot air streams at T-junction experimentally (Re $\approx 10^4$). Their major focus is the heat transfer between the inlet flows, so only some flow characteristics are discussed in their paper. They also found that the highest turbulent fluctuations occur at the edge of the recirculating zone. To the authors' knowledge, there is a study related to the noise generation of merging flow at duct junction (Karlsson *et al.*[4]) in which only the calculating

a)Author to whom correspondence should be addressed. Electronic mail: mmrleung@polyu.edu.hk

method of the strength of T-junction acoustic source is mentioned, but no explicit results are given in their work because their focus is on the aeroacoustic response of the T-junction.

The flow unsteadiness due to merging at T-junction is not fully investigated, nor is its associated noise generation. This is expected to be very significant in many practical applications in which the Reynolds number based on the duct width and the inlet flow speed is larger than 10^4. The aim of this paper is to study the aeroacoustics of the high Reynolds number ($\sim 10^5$) flow merging at T-junction. The characteristics of the noise generation are explored. However, it is not the objective of this paper to give the full details about the dynamics of merging flow. The primary focus is the relationship between noise-generating flow mechanisms and the noise produced. In particular, the effect of the velocity ratio between two inlet flows on the aeroacoustics is highlighted.

As a starting point in this study, two-dimensional calculations based on direct aeroacoustic simulation (DAS) approach are adopted. Notwithstanding the simplicity of this approach, the key noise generating flow dynamics can still be extracted from the solutions. Firstly, a brief of the numerical method and turbulence modeling adopted for the DAS is provided in Sec. II, followed by a description of the problem in Sec. III. In Sec. IV, an evaluation of DAS solver capability is provided. The flow dynamics and the acoustic generation interpreted from the numerical results at various velocity ratios are presented and discussed. One has to realize the fact that the extraction of acoustic signals from an unsteady flow is a difficult task even non-intrusive flow measurement technique, such as particle image velocimetry (PIV), is used. To circumvent this difficulty, a method for extracting the acoustics from DAS solutions is proposed and attempted in the section.

II. DIRECT AEROACOUSTIC SIMULATION

In essence, DAS is a numerical approach that simultaneously calculates both the acoustic field and the unsteady flow generating it by solving the unsteady compressible Navier-Stokes (N-S) equations and the equation of states. Thus, coupling between these two fields is inherently accounted for. This capability is important in determining the aeroacoustics of internal flows because the acoustic fluctuations are reflected by the duct walls and mixed with the flow fluctuations in the duct. This is different from the acoustic generation by an external flow, whereas the acoustics are allowed to propagate to the far field without affecting the flow dynamic source in the near field. Hybrid approach such as acoustic analogy can be directly applied to calculate the acoustic far field in these cases. Nevertheless, this method may not be applicable to the internal flow due to the lack of the coupling between acoustic and flow fields. In this sense, DAS is a better choice for the study of the acoustic generation of internal flow. Many successful applications of DAS have been reported in the investigations of the aeroacoustics of external and internal flows.[7–10]

The DAS solver must be capable of accurately calculating the acoustic and flow fluctuations, which exhibit large disparity in their energy and length scales. This poses strict requirements to the solver of being low dissipation and highly accurate. Conventionally, high order finite difference schemes such as Bogey[11] are adopted in DAS. Recently, the conservation element and solution element (CE/SE) method[12] has been proven to be a viable alternative. This numerical scheme takes an entirely different approach and concept from conventional schemes (e.g., finite-difference). Its construction of numerical framework relies solely on strict conservation of physical laws and emphasis on the unified treatment in both space and time. Much research has attempted the CE/SE method in solving various compressible flow problems such as unsteady viscous and Euler flows, traveling and interacting shocks, and supersonic jet noise.[13] Lam[14] further established that CE/SE method is capable of resolving the interactions between the unsteady flow and acoustic field accurately by calculating the benchmark aeroacoustic problems with increasing complexity. Therefore, the CE/SE method is adopted as the DAS solver in the present study. In this paper, the formulation of the CE/SE method is not given. Its details can be referred to in the works of Lam.[14]

A. Governing equations

The current aeroacoustic problem is governed by the two-dimensional compressible N-S equations together with ideal gas law for calorically perfect gas. Since the Reynolds number of most practical flows is high ($>10^5$) as a result of the high flow speed and large dimension, the flow is often turbulent. Large eddy simulation (LES) is applied to the N-S equations for accounting the effects of flow turbulence. In the following discussion, the pressure p, the density ρ, the temperature T, and the heat q are spatial filtered variables, while all other variables are the Favre variables (density weighted). Furthermore, the variables with a caret "^" denote the variables with dimensions. Taking the reference scales such as length $\hat{L}_o$, velocity $\hat{u}_o$, time $\hat{t}_o$, $\hat{\rho}_o$, $\hat{\rho}_o\hat{u}_o^2$, $\hat{T}_o$, and $\hat{\mu}_o$ from the problem, the non-dimensionalized N-S equations in two dimensions without source can be written in strong conservation form as

$$\frac{\partial \boldsymbol{U}}{\partial t} + \frac{\partial(\boldsymbol{F} - \boldsymbol{F}_v)}{\partial x} + \frac{\partial(\boldsymbol{G} - \boldsymbol{G}_v)}{\partial y} = \mathrm{SGS}, \tag{1}$$

where

$$\boldsymbol{U} = \begin{bmatrix} \rho \\ \rho u \\ \rho v \\ \rho E \end{bmatrix}, \quad \boldsymbol{F} = \begin{bmatrix} \rho u \\ \rho u^2 + p \\ \rho uv \\ (\rho E + p)u \end{bmatrix}, \quad \boldsymbol{G} = \begin{bmatrix} \rho v \\ \rho uv \\ \rho v^2 + p \\ (\rho E + p)v \end{bmatrix},$$

$$\boldsymbol{F}_v = \frac{1}{\mathrm{Re}} \begin{bmatrix} 0 \\ \tau_{xx} \\ \tau_{xy} \\ \alpha_x \end{bmatrix}, \quad \boldsymbol{G}_v = \frac{1}{\mathrm{Re}} \begin{bmatrix} 0 \\ \tau_{xy} \\ \tau_{yy} \\ \alpha_y \end{bmatrix},$$

with u and v being the normalized velocities in x and y direction, respectively, $\alpha_x = \tau_{xx}u + \tau_{xy}v - q_x$, $\alpha_y = \tau_{xy}u + \tau_{yy}v - q_y$, $\tau_{xx} = (2/3)\mu(2(\partial u/\partial x) - (\partial v/\partial y))$, $\tau_{xy} = \mu(\partial u/\partial y + \partial v/\partial x)$, $\tau_{yy} = (2/3)\mu(2(\partial v/\partial y) - (\partial u/\partial x))$, $E = p/\rho(\gamma - 1) + (u^2 + v^2)/2$, $p = \rho T/\gamma M^2$, $q_x = -[\mu/(\gamma - 1)\mathrm{Pr}M^2]$

$(\partial T/\partial x)$, $q_y = -[\mu/(\gamma-1)\mathrm{Pr}M^2](\partial T/\partial y)$, the specific heat ratio $\gamma = 1.4$, Mach number $M = \hat{u}_o/\hat{c}_o$, $\hat{c}_o = \sqrt{\gamma \hat{R}\hat{T}_o}$, the specific gas constant for air $\hat{R} = 287.058\ \mathrm{J/(kg \cdot K)}$, Reynolds number $\mathrm{Re} = \hat{\rho}_o \hat{u}_o \hat{L}_o/\hat{\mu}_o$, and Prandtl number $\mathrm{Pr} = \hat{c}_{p,o}\hat{\mu}_o/\hat{k}_o = 0.71$. The subgrid scale terms (SGS) represent all the terms adopted in the subgrid scale model in the LES.[8]

B. Large eddy simulation

Many approaches have been proposed for the turbulent modeling in literature,[15] e.g., URANS (unsteady Reynolds-averaged Navier-Stokes simulation), LES. Since URANS mainly captures the mean behaviors of a turbulent flow,[15] it is not suitable for the present study because noise-generating flow fluctuating behaviors cannot be fully resolved. The LES approach appears to be a better choice for the study of the aeroacoustics.[15] An efficient type of LES, MILES (monotonically integrated large eddy simulation)[16] is adopted in the present study. This approach utilizes the dissipation of a numerical scheme to mimic the actual turbulent dissipation in the flows; thus, any subgrid scale model is not invoked, i.e., setting SGS = 0 in Eq. (1). Lots of researchers have already demonstrated the success of MILES in obtaining different turbulent flow solutions. For example, Fureby[17] applied MILES to study the free shear jet ($\mathrm{Re} = 8.5 \times 10^4 \sim 2.2 \times 10^5$) and channel flow ($\mathrm{Re} \sim 10^4$). In this work, the dominant fluid dynamic fluctuations agreed well with those obtained from experiments and direct numerical simulation (DNS). Another example is the turbulent flow passing a backward facing step[8] in which not only the fluctuating velocity and the Reynolds stresses, but also the flow structures deduced by MILES showed a good agreement with those observed in experiments and other LES solutions. Furthermore, MILES was adapted to CE/SE method in the study of the gap noise of automobile body,[18] where the resonant frequency of the flow is correctly captured. All these studies show that the CE/SE method with MILES is a good choice for calculating the aerodynamics and aeroacoustics of turbulent flow. In order to further relax the mesh requirement of the LES, a wall modeling accommodating the viscous effect near the wall is also applied in the present study. This model introduces an additional viscous dissipation caused by the wall in the regions adjacent to the wall. The wall modeling is based on the classical logarithm law of wall with van Driest compressibility correction.[19] The friction velocity u_τ is first determined by an iterative Newton process with the known u adjacent to the wall. Then, the turbulent viscous dissipation is estimated from u_τ.

III. FORMULATION OF FLOW PROBLEM

The computational domain of a T-junction is illustrated in Fig. 1, and the reference parameters adopted are given in Table I. The non-dimensional lengths of all branches are set equal to 20 for ensuring sufficient space for the generated noise to propagate. The flow enters the domain through duct inlets I_1 (main flow) and I_2 (side flow). The merged flow leaves the computational domain through the outlet on the right. Furthermore, the typical Mach number $M = 0.1$ and

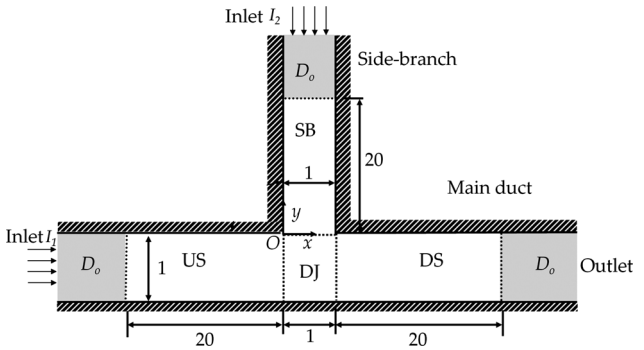

FIG. 1. Schematic of the merging flow problem. All parameters indicated are non-dimensionalized using the parameters in Table I. The origin O is located at the upstream corner of the duct junction. US: upstream branch (branch 1); SB: side branch (branch 2); DS: downstream branch (branch 3); DJ: duct junction.

the Reynolds number $\mathrm{Re} = 2.3 \times 10^5$ of a ventilation system are adopted in the present study. To aid the forthcoming discussions, four regions, namely US (upstream branch), SB (side branch), DJ (duct junction), and DS (downstream branch), are defined (Fig. 1).

The mesh is designed to meet the requirements for turbulent flow simulation. The mesh points are clustered near all the walls and relaxed toward the center line of the duct. The maximum mesh size $\Delta x_{\max} = 0.015$ at the center of the duct and its minimum $\Delta x_{\min} = 0.001$ at the walls. $\Delta x_{\min}$ corresponds to the wall unit, $y^+ = y\rho_w u_\tau \mathrm{Re}/\mu_w = 16$ at $M = 0.1$, where u_τ is the friction velocity, ρ_w is the fluid density at wall, and μ_w is the fluid viscosity at wall. There are roughly 20 meshes inside each turbulent boundary layer. Even at the maximum flow speed $M = 0.2$ considered in the present study, there are 16 mesh points inside each turbulent boundary layer. Such mesh distribution ensures that the developments of boundary layers are sufficiently captured.

In each calculation, an approximate time stationary solution obtained from a separate calculation on a coarser mesh is taken as the initial condition. Afterward, the calculations are proceeded with a duration of 40 so as to obtain a time stationary solution with the range of time increment, $5 \times 10^{-4} \le \Delta t \le 6.25 \times 10^{-4}$ for all cases.

Ghost cell approach is adopted for the specification of boundary condition in the CE/SE method. All duct walls are the no-slip wall boundary condition[14] (NSWBC-NW) given by

$$\rho_g = \rho_o, \quad p_g = p_o, \quad u_g = u_w, \quad v_g = v_w, \tag{2}$$

and

$$(\boldsymbol{U}_x)_b = (\boldsymbol{U}_x)_g, \quad (\boldsymbol{U}_y)_b = (\boldsymbol{U}_y)_g, \tag{3}$$

TABLE I. Definitions of reference parameters.

Reference parameters	Physical variables
Length, $\hat{L}_o$	Height of duct, $\hat{H}$
Velocity, $\hat{u}_o$	Maximum velocity at I_2, $\hat{u}_{2,\max}$
Time, $\hat{t}_o$	$\hat{H}/\hat{u}_{2,\max}$
Density, $\hat{\rho}_o$	Density at inlets, $\hat{\rho}_{\mathrm{in}}$
Pressure, $\hat{\rho}_o \hat{u}_o^2$	Inlet pressure $\hat{\rho}_{\mathrm{in}}\hat{u}_{2,\max}^2$

where the subscript b, g, and o denote the boundary cell, the ghost cell, and the reference state respectively, and u_w and v_w are the velocities of the wall. The wall modeling for turbulent flow is also applied to NSWBC-NW. Moreover, nonreflecting boundary condition[20] (NRBC) is applied to duct outlet. The specification of NRBC is similar to that of NSWBC-NW except the velocities as $u_g = u_b$ and $v_g = v_b$. Moreover, a numerical anechoic termination is applied to the inlets and outlet of the T-junction. The anechoic termination is composed of a buffer and the NRBC at the zone inflow/outflow boundary of the inlet/outlet. Gradual stretching of meshes in the buffer zones, D_I and D_o each of length 10, acts to absorb waves leaving the T-junction computational domain before they are eliminated by the NRBC at domain boundaries. Such specification was shown successfully minimizing the wave reflection in different aeroacoustics simulations.[13,14,18] The quality of the anechoic termination is established by injecting weak acoustic waves (amplitude -10^5) into the DS and calculating the reflection coefficients at the entrance of the buffer zone D_o. Within the range of frequency of interest ($f > 0.4$), the reflection coefficient is less than 0.073% and decays rapidly to zero at $f = 1$, which is the cutoff frequency of the duct. Therefore, practically there is no wave reflected from the duct inlet and outlets. At the two inlet flows, fully developed turbulent velocity profiles are specified. They are given by the classical logarithmic law, i.e., $u^+ = (1/k)\ln y^+ + C$, where $u^+ = u/u_\tau$, $\kappa = 0.41$, and $C = 5.0\tilde{u}_\tau$ is estimated by solving this equation with ρ_w, μ_w, and u at $y = 0.5$. Though this law is derived originally for the incompressible flow, it also serves as a good approximation in the present problem because the Mach numbers in the present study are below the compressibility limit ($M = 0.3$). In addition, no flow disturbance is introduced at the duct inlets.

In the present study, the velocity ratio VR between two inlet flows is defined as

$$VR = \frac{\hat{u}_{2,\max}}{\hat{u}_{1,\max}} = \frac{u_{2,\max}}{u_{1,\max}}, \tag{4}$$

where $\hat{u}_{1,\max}$ and $\hat{u}_{2,\max}$ are the maximum velocity at inlet I_1 and I_2, respectively. The VR simulated are 0.5, 0.67, 1.0, and 2.0.

IV. RESULTS AND DISCUSSIONS

A. Evaluation of the capability of CE/SE method

Before analyzing the merging flow aeroacoustics, the capability of CE/SE method in resolving the key aeroacoustical physics needs to be verified with existing literature. Since the literature focusing on the merging flow at T-junction is rare, the grazing flow at T-junction under acoustic excitation has been widely studied so it is chosen for the verification. In addition, calculations of merging flow described in the work of Hofmans[21] further establish the capability of CE/SE method in producing correct aeroacoustic solution.

1. Grazing flow

In the work of Martinez-Lera *et al.*,[3] the aeroacoustic response of a T-junction was investigated numerically. A steady incompressible base flow in the main duct was first obtained in the absence of flow in side branch. An acoustic wave was then excited in the different duct branches. These results were finally analyzed for determining the aeroacoustic response. For the present verification, only their a3 configuration, which concerns the aeroacoustic response with an excitation in SB, is attempted here. The length of US, SB, and DS are $3H$, $3H$, and $9H$ respectively, where H is the duct width. A uniform flow with speed u_1 is supplied at inlet I_1. All the walls are specified with NSWBC-NW and the outflow takes NRBC. The base flow is obtained from a simulation of time $t_b = 100\,H/u_1$, and then acoustic wave with speed $u' = 0.2u_1$, and different frequency f is excited at outlet 2. The simulations of these acoustic excitations are carried out for a time period of $t_a = 10\,H/u_1$.

Figure 2 shows the comparison of the present CE/SE results with those from existing literature. Here the acoustic power W is determined by following the procedures described in the work of Martinez-Lera *et al.*[3] except that the central part of the duct excluding the duct boundary layers, rather than the entire duct cross section, is chosen for calculating the area-averaged pressure to avoid the contamination of boundary layer induced fluctuations. The Strouhal number here is defined as $\mathrm{St} = fH/u_1$. It shows that the CE/SE results agree favorably with the trend of all other results. They also match the experimental results by Graf and Ziada[22] better than the quasi-steady one-dimensional model. This illustrates that the CE/SE method can capture the acoustic-flow interaction very well and is suitable for the present study.

2. Merging flow

In the context of Hofmans's study[21] on the acoustic generation of T-duct, the present merging flow can be considered as one of his cases with acoustic inflow u' (i.e., u'_2 in Fig. 2). In his work, a one-dimensional quasi-steady model is derived for estimating the acoustic source pressure ΔP_s for

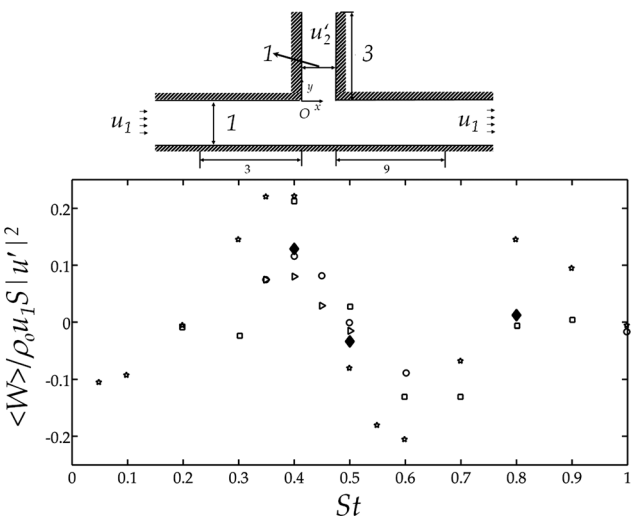

FIG. 2. Variation of normalized average acoustic power with Strouhal number of a3 configuration with grazing flow. ⋆, Hofmans quasi-steady model; ◆, CE/SE results; □, Martínez-Lera *et al.*; ○, Graf and Ziada (Ref. 22; Experiment $u' = 0.14$); ∇, Graf and Ziada (Ref. 22; Experiment $u' = 0.25$).

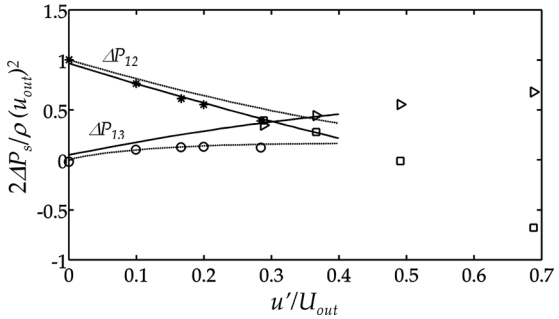

FIG. 3. Acoustic source pressure $\Delta P_{s,12}$ and $\Delta P_{s,13}$. —, experiments (Ref. 23); – –, one-dimensional quasi-steady model. ΔP_{12} : ▷, CE/SE; ○, vortex blob model. ΔP_{13} : □, CE/SE; ∗, vortex blob model.

T-junction. For an inviscid flow, it is defined as the total pressure jump across the T-junction, i.e.,

$$\Delta P_{s,ij} = P_i - P_j, \tag{5}$$

where i and j are the indices of the section in different duct branches. For practical flows, the correction of friction due to viscous effect on duct walls is required and is based on estimation of the total pressure loss in the duct. Vortex blob method was also applied under the assumption of quasi-steady model to account for the flow separation in Hofmans's work. Figure 3 shows a comparison of CE/SE results with those obtained from experiments[23] and Hofmans's models. Here $\Delta P_{s,12}$ is the acoustic source pressure between US and SB while $\Delta P_{s,13}$ is that between US and DS. The CE/SE pressure jumps averaged across duct cross sections are calculated for a better comparison with one-dimensional theory. Evidently, the CE/SE results match the trend of all other results favorably well, especially the experimental results. The noticeable discrepancy between the CE/SE results and Hofmans's is possibly due to the simplified assumption in the latter. Furthermore, CE/SE results outline a smooth trend even beyond $u'/U_{\text{out}} > 0.4$ though experimental results are not available in this range.

B. Flow dynamics

1. Grid convergence

For all cases attempted in the paper, grid convergence is fully established before the actual calculations. For illustrative purpose, only grid convergence check with case $VR = 1.0$ is described here. The mesh constructions are summarized in Table II. All calculations are allowed to proceed to a time $t = 10$. Figure 4 shows the sensitivity of resolved temporal development of pressure at different duct locations. It is found that the variation decreases with the mesh size. Only slight deviations are observed comparing the results of Mesh A and Mesh B while those between Mesh A and Mesh C are more noticeable. Both the large and small scales of the pressure fluctuations captured by Mesh A and Mesh B are essentially the same, so this indicates the convergence of the results in the calculations. In all the following discussions of merging flow aeroacoustics, the results are calculated with Mesh B.

TABLE II. Mesh constructions.

Meshes	Mesh sizes
A	$\Delta x_{\min} = 0.0005$, $\Delta x_{\max} = 0.015$, $\Delta t = 1.25 \times 10^{-5}$
B	$\Delta x_{\min} = 0.001$, $\Delta x_{\max} = 0.03$, $\Delta t = 2.5 \times 10^{-5}$
C	$\Delta x_{\min} = 0.002$, $\Delta x_{\max} = 0.06$, $\Delta t = 5 \times 10^{-5}$

2. Mean flows

Figures 5(a), 5(c), 5(e), and 5(g) illustrate the mean velocities in x-direction, u_{mean}, along different cross sections in the main duct for all four VRs. Generally, u_{mean} keeps the fully developed turbulent profile at $x < 0$ (US). Then, the u_{mean} profiles start to deform on approaching DJ ($x = 0$). The two inlet flows merge in DJ, leading to the formation of recirculating zones at both the upstream and downstream edges of DJ. Owing to the existence of these recirculating zones, the flow is accelerated at $x > 1$. Meanwhile, the boundary layers (BL) near the lower wall are squeezed to very thin layer in this region. Finally, the velocity profiles recover to a symmetric profile further downstream in DS.

In general, three different flow features can be readily observed by inspecting the mean vorticity ω_{mean} near DJ as shown in Figs. 5(b), 5(d), 5(f), and 5(h), on which streamlines are also presented. The first one is the recirculating zone RZ1 created at the downstream edge of DJ; the second one is the curved shear layer (SL) generated between the two merging flows in DJ; further upstream of SL, the last flow feature observed is another recirculating zone RZ2 at the upstream edge of DJ. Such a kind of flow regime is similar to that reported in previous literature.[6] Among these features, RZ1 contains the highest vorticity. Therefore, it is expected to be the major source of flow unsteadiness.

3. Flow unsteadiness

Figure 6(a) shows that the mean resolved Reynolds shear stress $\overline{u'v'}/u_{\text{eq}}^2$ over the domain, where the overbar denotes the time averaged variable, the superscript "′" denotes the fluctuating quantities as defined by

$$\phi'(x, y, t) = \phi(x, y, t) - \overline{\phi}(x, y), \tag{6}$$

with ϕ denoting the flow variables u, v, and

$$u_{\text{eq}}^2 = u_{1,\max}^2 + u_{2,\max}^2. \tag{7}$$

This figure shows that the region near RZ1 contains the highest Reynolds shear stress. This suggests that localized strong flow fluctuations occur there. In US and SB, the stress levels are significantly lower. Even at region near SL, the stress level is rather low compared with that at region near RZ1. This indicates that the flow unsteadiness of all VR is dominated by those at RZ1. Furthermore, the stress level increases with VR, leading to the highest stress level at $VR = 2$, implying very strong flow fluctuations at this VR. Similar stress distribution and variation with VR are also observed for $\overline{u'u'}/u_{\text{eq}}^2$ and $\overline{v'v'}/u_{\text{eq}}^2$, so they are not shown here. This also demonstrates that the merging flow fluctuations are localized downstream near the junction ($x < 10$).

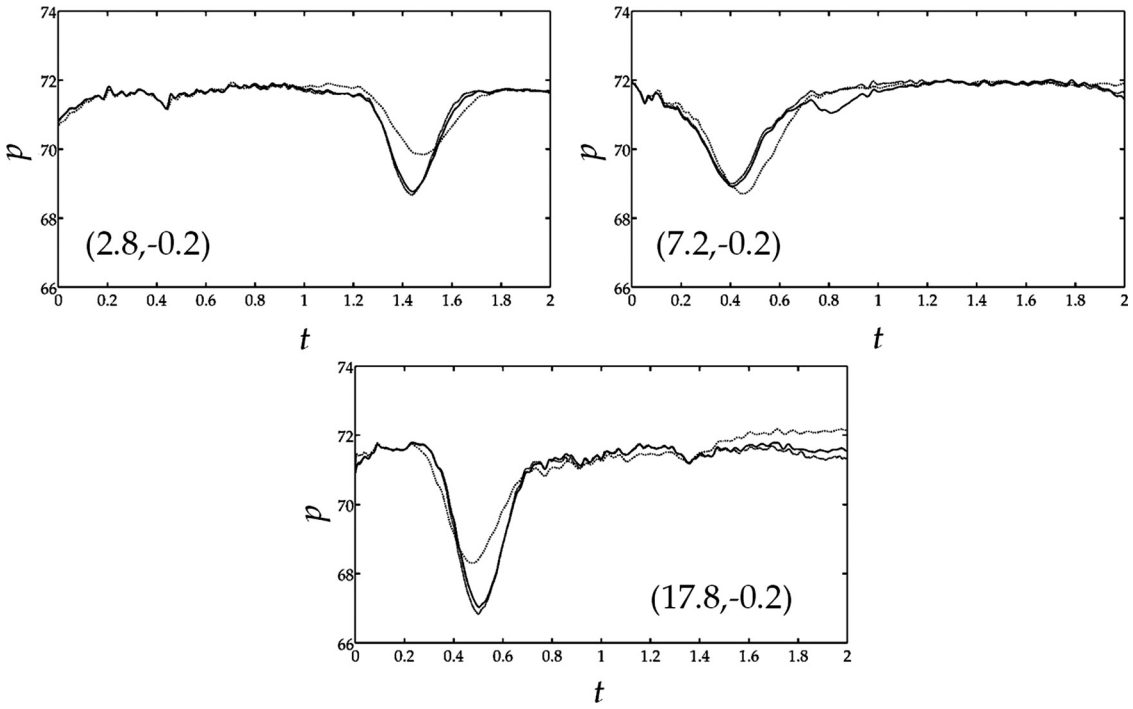

FIG. 4. Sensitivity of resolved temporal development of pressure to mesh size. - -: Mesh A; -: Mesh B; · · ·: Mesh C. Upper left: at $(x,y) = (2.8,-0.2)$; upper right: at $(x,y) = (7.2,-0.2)$; bottom: at $(x,y) = (17.8,-0.2)$.

Hence, the discussion on the flow dynamics is focused near the junction.

Figure 6(b) shows the snapshots of instantaneous vorticity for all *VR* cases. In general, the flow unsteadiness can be categorized into two solutions. In the first category ($VR < 1$), vortex roll-up at SL and rather large vortex shedding at RZ1 are observed. The vortex shed from the separated flow at RZ1 (e.g., vortex *a* at $VR = 0.5$) interacts and engulfs the vortex rolled up at SL (e.g., vortex *b* at $VR = 0.5$). The resultant vortex after interaction is convected toward the lower wall and then bounces back to the upper wall (e.g., vortex *c* at $VR = 0.5$). In the second category ($VR \geq 1$), the vortex shedding at RZ1 is still observed but there is no roll-up of the SL. However, the SL is entrained by the vortex shed at RZ1 to form a vortex (e.g., vortex *d* at $VR = 1.0$). In both categories, when the vortex shed at RZ1 approaches the lower wall, secondary vortices of opposite sense of rotation are induced at the lower wall (e.g., vortex *e* at $VR = 2.0$ formed by such interaction) and bounce between the walls. In general, the flow pattern becomes irregular as flow convects to downstream of the junction. When *VR* is increased, the irregularity in flow pattern in DS is increased possibly due to the increased occurrence of vortices. This explains the variation of mean Reynolds stresses with *VR* in Fig. 6. Figure 7 shows that spectra of pressure fluctuations at a location between $(2,-0.2)$ and $(3,-0.2)$ lying on the paths of the vortices shed at RZ1 for all *VR*'s. Increasing number of dominant peaks in the spectra are observed which also indicates the increasing complexity of the flow unsteadiness observed at T-junction as *VR* increases.

C. Acoustic generation

The connection between the flow unsteadiness and the acoustics can be inferred from the acoustic analogy.[24] For instance, the major source of flow induced acoustic generation in a open flow such as jet is fluctuating Reynolds stresses (quadruple type). For a low Mach number internal flow, the major acoustic source is attributed to the fluctuating forces exerted on the solid boundary (dipole type), rather than the fluctuating Reynolds stresses. Therefore, in the present study, the fluctuating wall pressure can be interpreted as an dominant acoustic source.

Figure 8(a) shows the total fluctuating wall pressure in all branches for $VR = 0.5$. The wall pressure is much higher in the DS than in the other two branches. This implies that the acoustic generation mainly arises from the branch DS. Similar behavior can also be observed in all other *VR*'s. The root mean square variation of the fluctuating wall pressure $(p'_{\text{wall}})_{\text{rms}}/\rho_o u_{\text{eq}}^2$ in DS is shown in Figs. 8(b) and 8(c). As *VR* increases, the level of $(p'_{\text{wall}})_{\text{rms}}/\rho_o u_{\text{eq}}^2$ also increases because of the stronger flow unsteadiness observed in the flow dynamics. The peak location on the upper wall corresponds to the location where the shedding of vortices occurs while that on the lower wall is the location where vortices collide. Since the vortices bounce in DS quite randomly, the distribution of $(p'_{\text{wall}})_{\text{rms}}/\rho_o u_{\text{eq}}^2$ is rather uniform after passing the peak location. This implies that the major actions generating the noise in merging flow are the formation of the vortical structures near the wall and the vortex bouncing at the wall. In Secs. IV C 1–IV C 4, the quantification of the acoustic generation associated is attempted.

1. Differentiation of acoustical and flow physics

One should bear in mind that the DAS solutions contain both the acoustic and flow dynamic fluctuations and their differentiation is not obvious. This fact creates a great difficulty in determining the dominant physics, whether acoustic

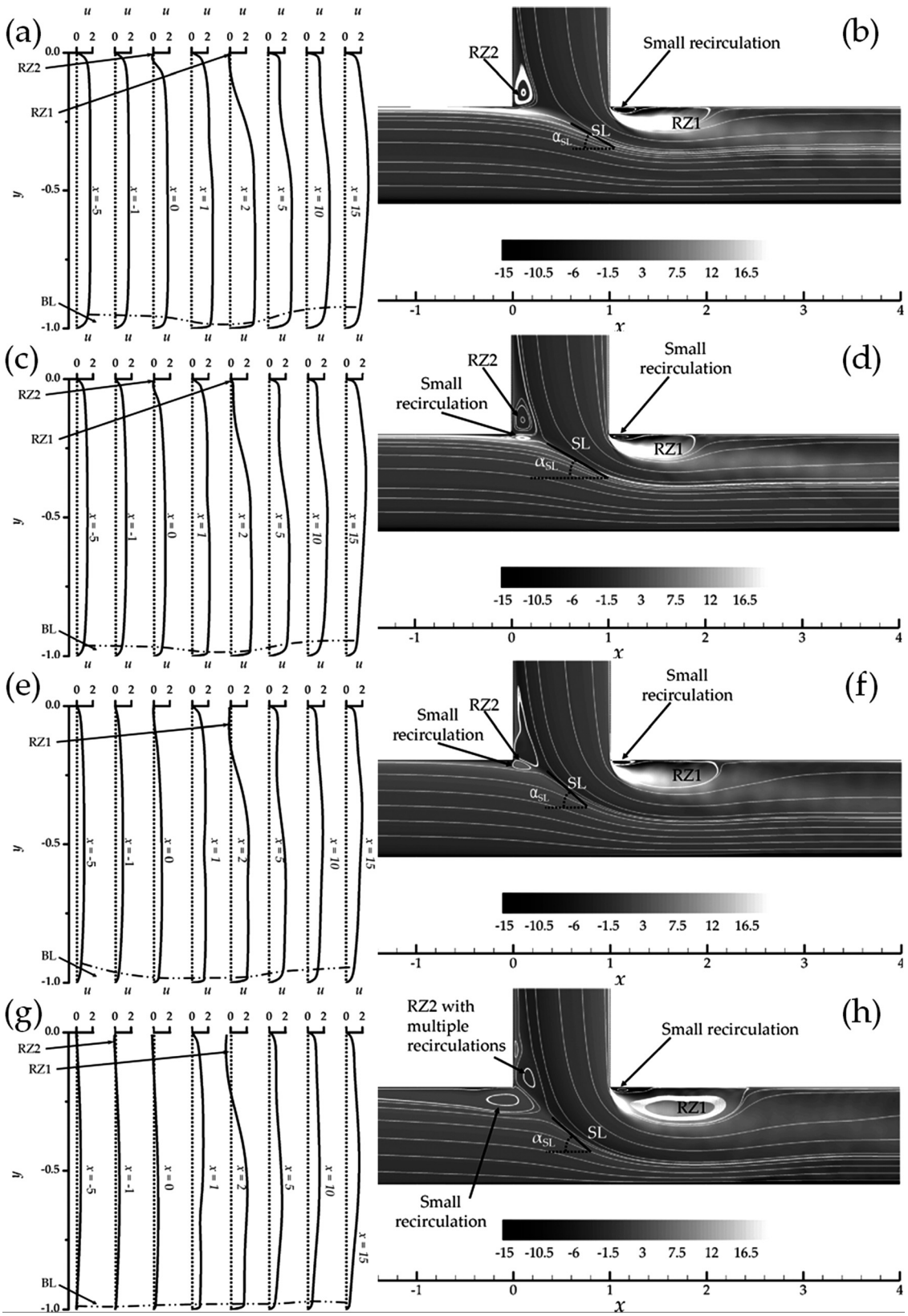

FIG. 5. Mean flow at various velocity ratios *VR*. The mean *x*-velocity profiles u_{mean} and mean vorticity ω_{mean} near the junction are shown in left and right columns, respectively. (a),(b) $VR = 0.5$; (c),(d) $VR = 0.67$; (e),(f) $VR = 1.0$; (g),(h) $VR = 2.0$.

or flow dynamic, in the solutions. It is especially true in regions where the acoustics is always generated by the underlying unsteady flow dynamics. In order to overcome this difficulty, a technique based on the principle of two-microphone method[10] is applied to differentiate the dominant physics in the junction merging flow. Consider a disturbance traveling through two locations, *P* and *Q*, separated by Δx in the flow. The phase difference ϑ_{PQ} of this

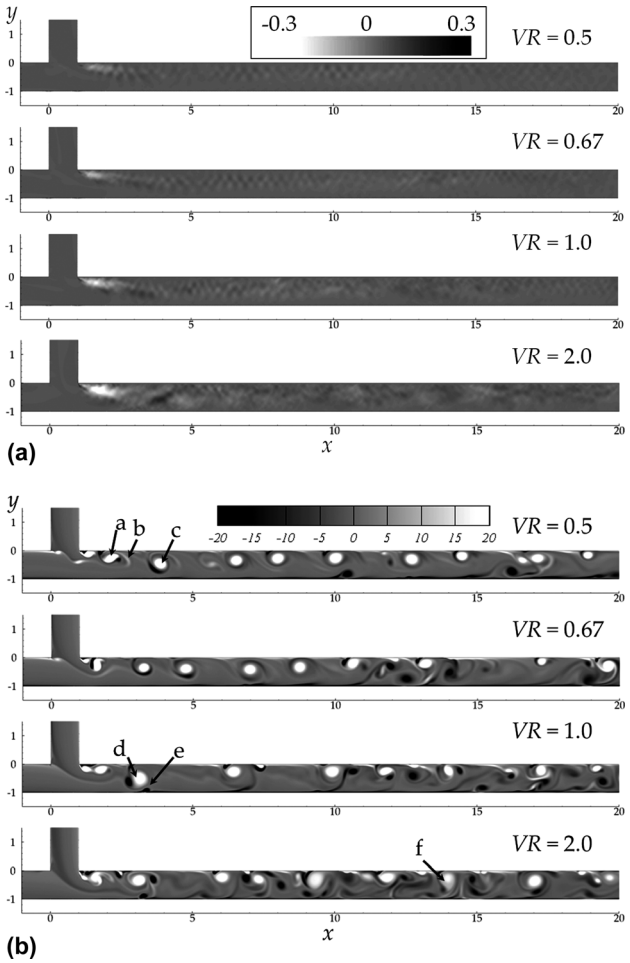

FIG. 6. Unsteady flow features. (a) Distributions of normalized Reynolds shear stress $\overline{u'v'}/u_{eq}^2$. (b) Snapshots of vorticity.

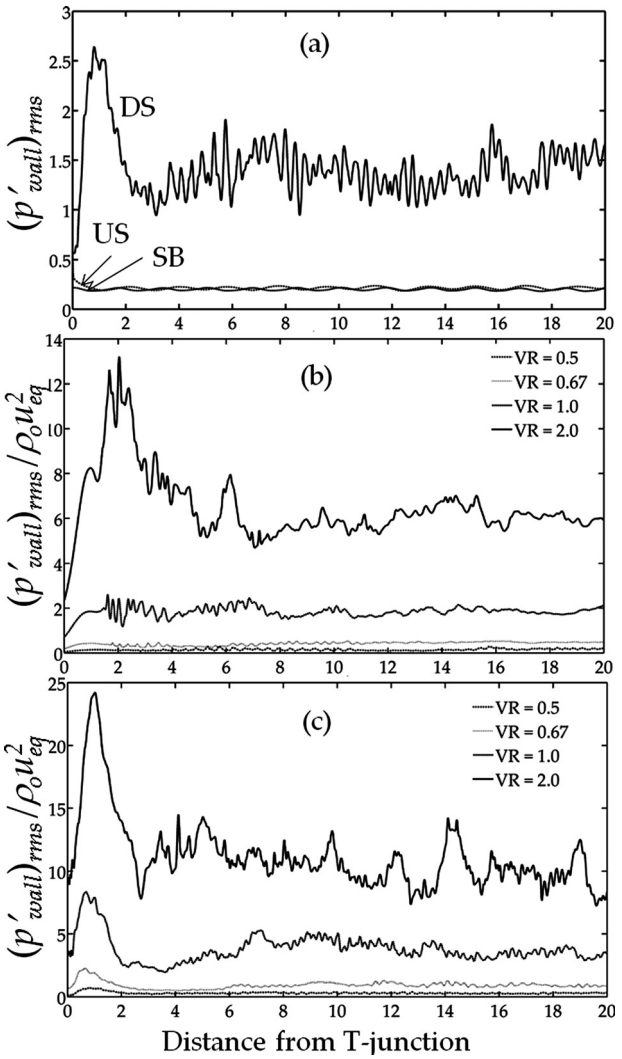

FIG. 8. (a) Distribution of total fluctuating wall pressure, $(p'_{wall})_{rms}$ in all branches at velocity ratio $VR = 0.5$ (DS: upstream branch, SB: side branch, DS: downstream branch), (b) $(p'_{wall})_{rms}/\rho_o u_{eq}^2$ at lower wall in DS, (c) $(p'_{wall})_{rms}/\rho_o u_{eq}^2$ at upper wall in DS.

disturbance between the individual phases ϑ_P and ϑ_Q is given by $\vartheta_{PQ} = \vartheta_P - \vartheta_Q$, where ϑ_P and ϑ_Q are obtained from fast Fourier transform analysis. When this disturbance passes through PQ with phase speed v_o, the theoretical phase difference for this disturbance ϑ_{PQ,v_o} can be expressed as

$$\vartheta_{PQ,v_o} = k_{v_o}\Delta x, \tag{8}$$

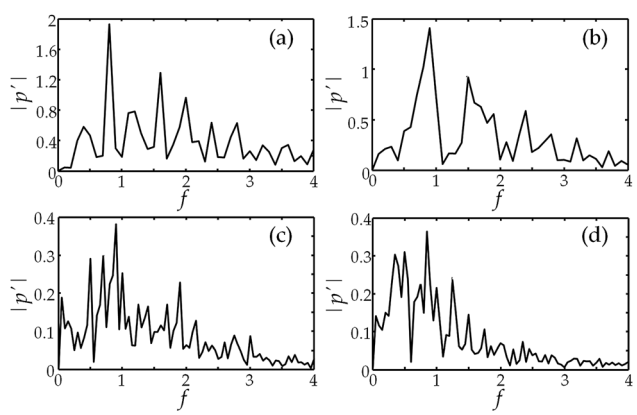

FIG. 7. Spectra of pressure fluctuation calculated at a location between (2,−0.2) and (3,−0.2) for all velocity ratios VR. (a) $VR = 0.5$; (b) $VR = 0.67$; (c) $VR = 1.0$; (d) $VR = 2.0$.

where $k_{vo} = 2\pi f/v_o$ is the wave number of the disturbance and f is the frequency of the disturbance. Therefore, the theoretical phase difference for an acoustic disturbance (c_o) and a flow disturbance (u_o) are given by

$$\vartheta_{PQ,c_o} = k_{c_o}\Delta x, \tag{9}$$

and

$$\vartheta_{PQ,u_o} = k_{u_o}\Delta x = \frac{1}{M}\vartheta_{PQ,c_o}, \tag{10}$$

respectively. Equation (10) shows that when $M \ll 1$, $\vartheta_{PQ,u_o} \gg \vartheta_{PQ,c_o}$, and the inequality allows a differentiation between acoustic and flow disturbances. Moreover, this method is especially efficient in low Mach number flows due to the vast difference in the characteristic speed of flow and the acoustic speed. If the acoustic disturbances dominate a region, then $\vartheta_{PQ} \to \vartheta_{PQ,c_o}$, and the acoustic effect is the dominant physics in that region. Similarly, when the flow disturbance is dominant in a region, $\vartheta_{PQ} \to \vartheta_{PQ,u_o}$, the flow unsteadiness dominates in that region.

Figure 9 shows that ϑ_{PQ} along the centerline of US, SB, and DS for $VR = 1.0$ calculated with a spatial separation of $\Delta x = \Delta y = 0.2$. Reference lines of ϑ_{PQ,c_o} and ϑ_{PQ,u_o} are also plotted in Fig. 9 due to the possibility of $\pm x$ traveling direction of the disturbances. All values of ϑ_{PQ} in US and SB lie on the reference lines $\pm\vartheta_{PQ,c_o}$. This implies that US and SB are dominated by the acoustic disturbances. On the contrary, the values of ϑ_{PQ} in DS and DJ lies between $|\vartheta_{PQ,c_o}|$ and $|\vartheta_{PQ,u_o}|$. This shows that both acoustic and flow disturbances are dominant in DS and DJ. Other *VR* cases also have similar behavior and so their results are not shown here.

2. Extraction of acoustic contribution

Since the disturbances are mixed in DS, this leads to another challenge in analyzing the DAS results. Conventional methods for spectral analysis are not able to separate the acoustic and flow disturbances especially when the acoustics are generated by the underlying flow dynamics. Therefore, an approach utilizing the two-dimensional wave number to frequency spectrum[25] is proposed to extract the acoustic contribution in mixed disturbances.

The pressure fluctuating field $p'(x,t)$ [$\phi = p$ in Eq. (6)] along a straight line mesh with uniform mesh size Δx is first transformed to a wave number - frequency spectrum $p'(k_x,f)$ by

$$p'(k_x,f) = \frac{1}{2\pi}\int\int p'(x,t)W(x)e^{-i(k_x x+2\pi ft)}\,dxdt, \qquad (11)$$

where $W(x)$ is the window function, f is the frequency, $k_x = 2\pi f/v_p$ is the wave number, and v_p is the phase speed of the disturbances. The mesh is aligned with the dominant traveling direction of disturbances. Based on Eq. (11), the fluctuation with the same frequency but different propagating speeds is decomposed. When the phase speed of the disturbance increases, k_x decreases for the same frequency. Such spectral analysis has been successfully applied to the jet-noise experiment[25] for the disturbance differentiation. In the current simulations, the time histories are recorded in a uniform mesh at $y = -0.2$ and 0.5 with $\Delta x = 0.2$ in DS. The mesh lies on the trajectories of the vortices and cuts through RZ1. The window function $W(x) = 1$ is arbitrarily chosen for the present study.

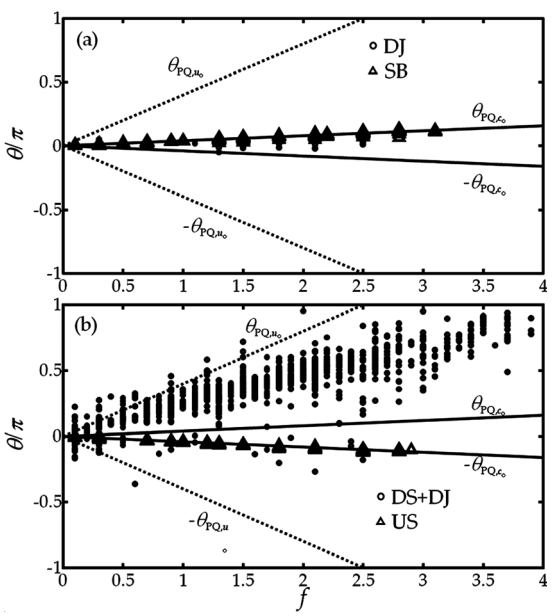

FIG. 9. Variations of phase difference θ along the selected lines ($VR = 1.0$). (a) Along the centerline of SB ($x = 0.5$, $y > 0$) and DJ ($x = 0.5$, $-0.6 > y > 0$). (b) Along the centerline of main duct ($x > 0$, $y = -0.5$). ○, the results in downstream branch DS and duct junction DJ; Δ, the results in side branch SB and upstream branch US.

Figure 10 shows the $(k_x - f)$ spectra divided by $\rho_o u_{eq}^2$ at $y = -0.2$ for all *VR* studied together with the loci of acoustic speed and other flow speeds. The region below the line $v_p = c_o$ is regarded as the incompressible zone because all the disturbances there travel with speeds higher than the speed of sound c_o (close to incompressible limit). On the other hand, the region above this solid line is regarded as the subsonic zone, whereas the disturbances propagate at subsonic speeds. Figure 10 indicates that the dominant disturbances in DS propagate with $v_p \sim 0.5 - 0.6u_m$, where $u_m = (u_{max} + u_{min})/2$. Here, u_{max} and u_{min} are, respectively, the maximum and minimum velocities in the separated flow at RZ1 and u_{min} is found to be zero. Moreover, when the dominant flow disturbances are filtered out, only the acoustic disturbances appear in the spectra, e.g., Fig. 10(e) with $VR = 1.0$ at $y = -0.2$. The relatively weak acoustic disturbances are clearly illustrated in this spectrum. Therefore, this two-dimensional Fourier transformation is capable of differentiating the mixed acoustic and flow dynamic signals in our DAS results and helping us to analyze the effects of individual disturbances passing through T-junction.

Such signal differentiation also facilitates the extraction of the acoustic contribution in the mixed disturbance energy inside DS. The $(k_x - f)$ spectra along the centerline of DS ($y = -0.5$) with $\Delta x = 0.2$ are first calculated. Integrations are then performed in the spectra within the areas A_{flow} and A_{acoust} marked in Fig. 10(e). These two areas are bounded by $v_{p,flow} \pm v_{tol}$ and $v_{p,acoust} \pm v_{tol}$, respectively, where $v_{tol} = 0.1$ is the tolerance applied, $v_{p,flow}$ and $v_{p,acoust}$ are the phase speeds of flow and acoustic disturbances, respectively. Thus, the contribution of acoustic component in mixed signals *AR* can estimated by

$$AR = A_{acoust}/(A_{acoust} + A_{flow}). \qquad (12)$$

Table III lists *AR* for different *VR*'s in this study. Evidently the acoustic contribution in all *VR* cases is 3 to 4 orders of magnitude smaller than the flow dynamic contribution. This disparity in acoustic and flow dynamic energy scales is typical in low Mach number aeroacoustics. *AR* can then be used to estimate the acoustic power when the overall fluctuating power is obtained.

3. Acoustic efficiency

The overall acoustic power generated W_{acoust} by a flow through a duct cross-section can be determined from the instantaneous acoustic intensity along that section.[10] When a mean flow is present, the instantaneous acoustic intensity $\mathbf{I}_a(t)$ at a point is given by

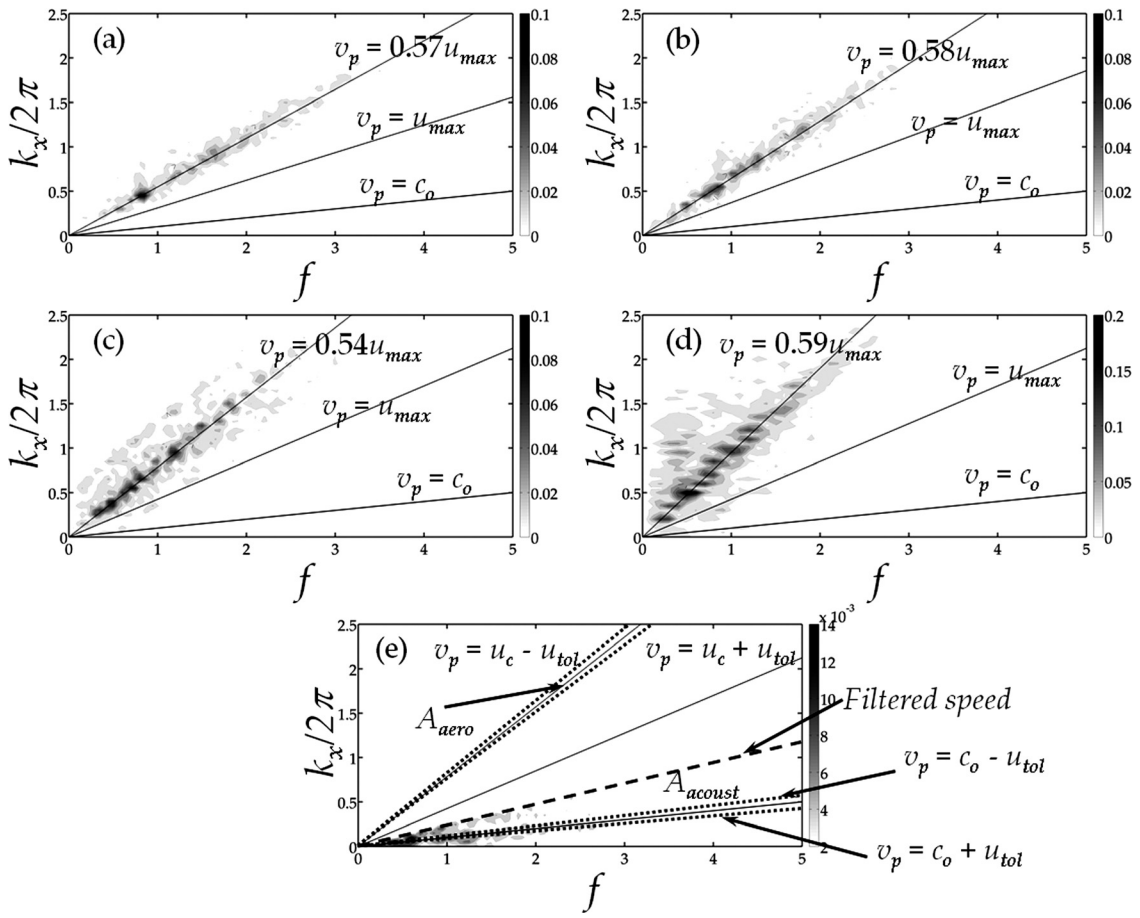

FIG. 10. Wave number - frequency ($k_x - f$) spectra normalized by $\rho_o u_{eq}^2$ at $y = -0.2$ in downstream branch DS for all velocity ratios *VR*. (a) $VR = 0.5$; (b) $VR = 0.67$; (c) $VR = 1.0$; (d) $VR = 2.0$; (e) filtered $k_x - f$ spectrum at $y = -0.2$ for $VR = 1.0$. v_p denotes the phase speed of the disturbances in duct.

$$\mathbf{I}_a(t) = p'\mathbf{u}' + (\mathbf{M}\cdot\mathbf{u}')(\mathbf{M}p' + \overline{\rho}c\mathbf{u}') + \mathbf{M}\left(\frac{p'^2}{\overline{\rho}c}\right), \qquad (13)$$

where c is the local acoustic speed, $\mathbf{u}' = (u', v')$ is the fluctuating velocities, p' is the fluctuating pressure, $\mathbf{M} = |\overline{\mathbf{u}}|/c$, $|\overline{\mathbf{u}}|$ is the mean velocity, and $\overline{\rho}$ is mean density. By integrating across the cross-section, the instantaneous acoustic power $W_i(t)$ per unit length is calculated by $W_i(t) = \int \mathbf{I}_a(t)\cdot\mathbf{n}\,ds$, where $\mathbf{n}$ is the unit outward normal of the section.[10] Unit thickness is assumed in the z direction in two dimensions. The overall acoustic power W_{acoust} is then given by $W_{\text{acoust}} = (1/T)\int_0^T W_i(t)\,dt$, where the duration T is usually chosen to cover at least one period of the lowest dominant frequency. The calculation of W_i should be done along a cross-section in the duct acoustic far field; otherwise, the results will represent the overall (acoustic + flow dynamic) fluctuations similar to the case in DS. In these calculations, the chosen cross-sections are $x = -9$ in US, $y = 9$ in SB, and $x = 10$ in DS. For each cross-section, the line integral only covers the region so chosen that the influence of duct boundary layer is excluded. Furthermore, in order to eliminate the bias of inlet flow variations on assessing acoustic generation capability in the different cases attempted, a term acoustic efficiency η is defined as

$$\eta = W_{\text{acoust}}/W_{\text{inlet}}. \qquad (14)$$

W_{inlet} is determined by $W_{\text{inlet}} = \sum_i \int (1/2)\rho(\mathbf{u}\cdot\mathbf{u})\ \mathbf{n}\cdot\mathbf{u}\,ds$, where i is the number of inlet duct section and $\mathbf{u}$ is the flow velocity. η essentially indicates the level of acoustic generation per unit flow power injected into the system. In DS, the acoustic efficiency is given by

$$\eta_{\text{DS}} = AR \times \eta_{\text{DS,overall}}, \qquad (15)$$

where $\eta_{\text{DS,overall}}$ is calculated from W_{acoust} and W_{inlet}.

It is found that the acoustic efficiency η increases with *VR* as shown in Fig. 11. In other words, the portion of the flow power input transformed to the acoustic power increases with *VR*. The observed trend in η may be explained with the flow unsteadiness in Fig. 6. Previous discussions have indicated that most noise generating flow unsteadiness mainly occurs around RZ1. At higher value of *VR* [e.g., $VR = 2.0$ in

TABLE III. Variation of the ratio of acoustic power to total power *AR* with velocity ratio *VR* in downstream branch DS.

VR	*AR*
0.5	2.42×10^{-4}
0.67	7.64×10^{-4}
1.0	6.88×10^{-4}
2.0	3.7×10^{-3}

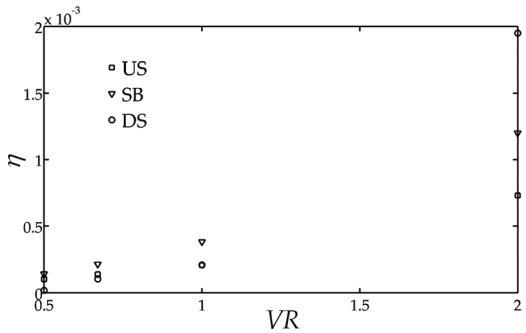

FIG. 11. Variation of acoustic efficiency η as a function of the velocity ratio VR for (□) the upstream branch US, (▽) the side branch SB, and (○) the downstream branch DS.

Fig. 6(b)], the unsteady vortical structures created at RZ1 appear to be larger and carrying higher circulation. Their interactions are stronger than their counterparts at low VR and the eventual noise generation is more effective. In fact the higher level of localized flow unsteadiness at $VR = 2.0$ is revealed in the distribution of mean Reynolds stress [Fig. 6(a)]. Thus, the noise production is enhanced when VR is increased. Generally, $\eta_{DS} < \eta_{US} \approx \eta_{SB}$. This may implies that the acoustic propagation in the merging flow has an upstream preference. For a source of dipole type in duct with mean flow, Åbom and Bodén[26] have derived an analytical expression for the acoustic power distribution in different branches, which also indicates an upstream preference in the acoustic propagation. This also agrees with Lighthill's analogy, which suggests a factor $(1 - \cos\theta)$ in the acoustic power under effect of mean flow, where θ is the direction. Since $\theta = 0°$ for downstream direction and $\theta = 180°$ for upstream direction, the acoustic power is greater in the upstream direction.

4. Acoustic scaling

In order to determine the relationship between the acoustic generation and the flow unsteadiness induced in the T-junction, an acoustic scaling is attempted in this paper. In previous research of noise generation by flow unsteadiness, a scaling between the flow velocity and the acoustic power is proposed, e.g., the famous u^8 scaling for jet by Lighthill.[27] According to Morfey,[28] the acoustic generation of a low Mach number internal flow generally involves two types of sources, namely, a quadruple-type and a dipole-type. In the work of Davies and Ffowcs-Williams,[29] the quadruple-type behavior in generation is caused by the turbulent fluctuations, i.e., the Reynolds stresses. They applied the one-dimensional duct Green's function in the acoustic analogy to deduce the acoustic power $W \propto \rho u_o^3 M_o^3$ generated by turbulence. Here u_o is the mean velocity of the flow and $M_o = u_o/c_o$ with reference sound speed c_o. This power exceeds that generated by the turbulence in external flow with same velocity u_o. With the total rate of flow input $W_{in} \sim \rho_o u_o^3 L_o^2$, where L_o is the characteristic length, the acoustic efficiency $\eta \propto M_o^3$. On the other hand, the dipole-type sources are usually associated with the flow induced forces on the interior solid surfaces F_{sur}.

Based on the work of Morfey,[28] the acoustic power W for a dipole-type source varies with the square of fluctuating F_{sur}. In the case of flow through a diaphragm in duct which is dominated by the dipole-type sources, Gloerfelt and Lafon[30] experimentally confirmed a u^4 scaling for the acoustic power generated. This observation suggests that the acoustic efficiency η scales with M_o. Upon normalizing the F_{sur} by $\rho_o u_o^2 L_o^2$, the acoustic efficiency η may take the scaling $\eta \propto (F_{sur}/\rho_o u_o^2 L_o^2)^2 M_o$. One should note that this is derived for the three-dimensional case. In two-dimensional low Mach number flow, Howe[31] suggested that the acoustic efficiency is further increased by M_o^{-1}. Therefore, for a quadruple,

$$\eta \propto M_o^2, \tag{16}$$

and for a dipole,

$$\eta \propto \left(\frac{F_{sur}}{\rho_o u_o^2 L_o^2}\right)^2. \tag{17}$$

In this paper, the scaling parameters F_{sur} and u_o are chosen to be the root mean square (RMS) of the fluctuating force F_{rms} on all the walls in DS and the averaged speed $u_{flow} = \sqrt{W_{inlet}/\rho u_{2,max}}$, respectively. F_{rms} is obtained by integrating the RMS of the fluctuating wall pressure in DS. The results are shown in Fig. 12. The exponent of acoustic efficiencies in the upstream branches (US and SB) is about 2. This indicates that in these two regions, the acoustic generation is of dipole type as suggested by Eq. (17). However, the exponent in downstream branch DS is about 3. This different exponent may be attributed to the different flow velocities in duct branches. It also indicates that the acoustic generation in DS is not purely of dipole type. Hu *et al.*[32] investigated the acoustic radiation in turbulent channel flows by applying acoustic analogy on the incompressible flow results obtained from DNS. They found that the acoustic generation in internal flow is generally dominated by both dipole- and quadrupole-type generation. It is observed that the quadruple generation starts to take over the dipole generation in the channel flow when the Mach number of the flow $M > 0.1$ for low frequency $f < 1$. In the present T-junction, the velocity at the downstream is increased due to the merging of the flows from its two upstream branches. This results in $M \sim 0.3$ in the downstream branch DS, which promotes the quadruple-type generation there as suggested by

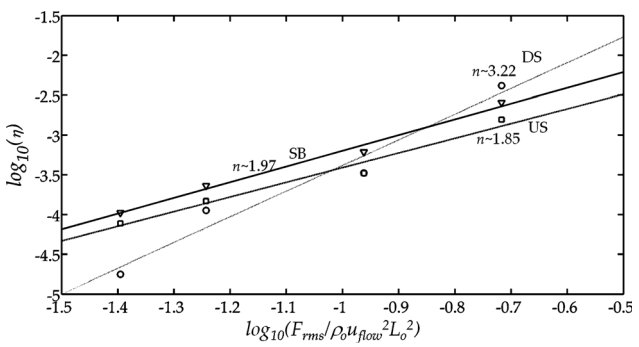

FIG. 12. Variation of acoustic efficiency η with the root mean squared value of normalized wall fluctuating force $(F_{rms}/\rho_o u_{flow}^2 L_o^2)$ · □, the upstream branch US; ▽, the side branch SB; ○, the downstream branch DS. n is the exponent obtained.

Hu *et al.*[32] In the meantime, the Mach number at the upstream branches is still at ~0.1, which suggests the dipole type generation at the upstream branches. This may explain the different exponents in the upstream and downstream branches observed in the acoustic efficiency.

V. CONCLUSIONS

A numerical study of aeroacoustics of two-dimensional merging flow at T-junction is reported. The focus of the study is to elucidate the acoustic generation by the flow unsteadiness which is seldom studied for a low Mach number duct flow. Direct aeroacoustic simulation with CE/SE method is adopted in the present study and MILES is applied in the turbulent modeling. The merging flow at duct junctions consists of three distinct flow features: the recirculating zone at downstream corner of duct junction, the shear layer between the two flows, and another recirculating region upstream of the duct junction. It is found that the vortex shedding at the flow region is the dominant flow unsteadiness due to the instabilities of the separated flow there. Furthermore, the acoustic source pressure is also correctly calculated by the CE/SE method. Since the acoustic and flow disturbances are mixed in the downstream of T-junction, a two-dimensional spectral analysis is applied to differentiate the disturbances. Based on these results, an approach for extracting the acoustic contribution in these regions is further proposed. Generally, the acoustic power generated increases with the velocity ratio of the flows between the main and side branch. The acoustic efficiency is found to be upstream biased, which agrees with the results reported in existing literature.[26] The fluctuating wall pressure in the downstream region of T-junction is found to be the major acoustic source. It is mainly caused by the shedding of the vortices from the duct junction and their subsequent collisions on the duct walls downstream. As such, an acoustic scaling between the fluctuating force and the acoustic efficiency is derived based on acoustic analogy to relate the acoustic generation and the flow unsteadiness. The scaling indicates that the acoustic generation in the upstream branches is of pure dipole type. However, the acoustic generation also exhibits additional quadrupole-type behavior in the downstream branch. This may be related to the increased velocity of the flow in the downstream branch, which enhances the quadruple generation there.

ACKNOWLEDGMENTS

Funding support received from the Research Grants Council of the HKSAR Government (through Grants Nos. PolyU 5278/06E and PolyU 5230/09E) and from the Hong Kong Polytechnic University (through Grant No. J-BB2C) are gratefully acknowledged.

[1]J. C. Bruggeman, A. Hirschberg, M. E. H. van Dongen, A. P. J. Wijnands, and J. Gorter, "Self-sustained aero-acoustic pulsations in gas transport systems: Experimental study of the influence of closed side branches," J. Sound Vib. **150**, 371–393 (1991).
[2]S. Dequand, S. J. Hulshoff, and A. Hirschberg, "Self-sustained oscillations in a closed side branch system," J. Sound Vib. **265**, 359–386 (2003).
[3]P. Martínez-Lera, C. Schram, S. Föller, R. Kaess, and W. Polifke, "Identification of the aeroacoustic response of a low Mach number flow through a T-joint," J. Acoust. Soc. Am. **126**, 582–586 (2009).
[4]M. Karlsson and M. Åbom, "Aeroacoustics of T-junctions—An experimental investigation," J. Sound Vib. **329**, 1793–1808 (2010).
[5]C. Brücker, "Study of the three-dimensional flow in a T-junction using a dual-scanning method for three-dimensional scanning-particle-image velocimetry (3-D SPIV)," Exp. Therm. Fluid Sci. **14**, 35–44 (1997).
[6]M. Hirota, E. Mohri, H. Asano, and H. Goto, "Experimental study on turbulent mixing process in cross-flow type T-junction," Int. J. Heat Fluid Flow **31**, 776–784 (2010).
[7]J. B. Freund, "Noise sources in a low-Reynolds-number turbulent jet at Mach 0.9," J. Fluid Mech. **438**, 277–305 (2001).
[8]L. Larchevêque, P. Sagaut, I. Mary, O. Labbé, and P. Comte, "Large-eddy simulation of a compressible flow past a deep cavity," Phys. Fluids **15**, 193–210 (2003).
[9]C. W. Rowley, T. Colonius, and A. J. Basu, "On self-sustained oscillations in two-dimensional compressible flow over rectangular cavities," J. Fluid Mech. **455**, 315–346 (2002).
[10]R. C. K. Leung, R. M. C. So, M. H. Wang, and X. M. Li, "In-duct orifice and its effect on sound absorption," J. Sound Vib. **299**, 990–1004 (2007).
[11]C. Bogey, "A family of low dispersive and low dissipative explicit schemes for flow and noise computations," J. Comput. Phys. **194**, 194–214 (2004).
[12]S. C. Chang, "The method of space-time conservation element and solution element—A new approach for solving the Navier-Stokes and Euler equations," J. Comput. Phys. **119**, 295–324 (1995).
[13]C. Y. Loh and L. S. Hultgren, "Jet screech noise computation," AIAA J. **44**, 992–998 (2006).
[14]G. C. Y. Lam, "Aeroacoustics of merging flow at duct junctions," Ph.D. thesis, The Hong Kong Polytechnic University (2012), pp. 1–204.
[15]*Large-Eddy Simulation for Acoustics*, edited by C. Wagne, T. Hüttl, and P. Sagaut (Cambridge University Press, Cambridge, New York, 2007), pp. 1–470.
[16]J. P. Boris, F. F. Grinstein, E. S. Oran, and R. L. Kolbe, "New insights into large eddy simulation," Fluid Dyn. Res. **10**, 199–228 (1992).
[17]C. Fureby, "Large eddy simulation of high-Reynolds-number free and wall-bounded flows," J. Comput. Phys. **181**, 68–97 (2002).
[18]C. Y. Loh, S. C. Chang, X. Y. Wang, and P. C. Jorgenson, "Gap noise computation by the CE/SE Method," NASA Technical Report NASA/TM-2001-210703 (2001), pp. 1–6.
[19]P. G. Huang, P. Bradshaw, and T. J. Coakley, "Skin friction velocity profile family for compressible turbulent boundary layers," AIAA J. **31**, 1600–1604 (1993).
[20]C. Y. Loh, "On a non-reflecting boundary condition for hyperbolic conservation laws," AIAA Pap. 2003-3975 1–28 (2003).
[21]G. Hofmans, "Vortex sound in confined flows," Ph.D. thesis, Technische Universiteit Eindhoven (1998), pp. 151–163.
[22]H. R. Graf and S. Ziada, "Flow induced acoustic resonance in closed side branches: An experimental determination of the excitation source," AMD (Am. Soc. Mech. Eng.) **151**, 63–80 (1992).
[23]H. Ito and K. Imai, "Energy losses at 90° pipe junctions," J. Hydr. Div. **99**, 1353–1368 (1973).
[24]N. Curle, "The influence of solid boundaries upon aerodynamic sound," Proc. R. Soc. London **231**, 505–514 (1955).
[25]C. E. Tinney and P. Jordan, "The near pressure field of co-axial subsonic jets," J. Fluid Mech. **611**, 175–204 (2008).
[26]M. Åbom and H. Bodén, "A note on the aeroacoustic source character of in-duct axial fans," J. Sound Vib. **186**, 589–598 (1995).
[27]M. J. Lighthill, "On sound generated aerodynamically. II. Turbulence as a source of sound," Proc. R. Soc. London **222**, 1–32 (1954).
[28]C. L. Morfey, "Sound transmission and generation in ducts with flow," J. Sound Vib. **14**, 37–55 (1971).
[29]H. G. Davies and J. E. Ffowcs-Williams, "Aerodynamic sound generation in a pipe," J. Fluid Mech. **32**, 765–778 (1967).
[30]X. Gloerfelt and P. Lafon, "Direct computation of the noise induced by a turbulent flow through a diaphragm in a duct at low Mach number," Comput. Fluids **37**, 388–401 (2008).
[31]M. S. Howe, *Acoustics of Fluid-Structure Interactions* (Cambridge University Press, Cambridge, 1998), pp. 107–108.
[32]Z. Hu, C. L. Morfey, and N. D. Sandham, "Sound radiation in turbulent channel flows," J. Fluid Mech. **475**, 269–302 (2003).